

Intraseasonal variability of latent-heat flux in the South China Sea

Lili Zeng · Dongxiao Wang

Received: 1 April 2008 / Accepted: 11 November 2008 / Published online: 1 April 2009
© Springer-Verlag 2009

Abstract Intraseasonal variability (ISV) of latent-heat flux in the South China Sea (SCS) is examined using 9 years of weekly data from January 1998 to December 2006. Using harmonic and composite analysis, some fundamental features of the latent-heat flux ISVs are revealed. Intraseasonal latent-heat flux has two spectral peaks around 28–35 and 49–56 days, comparable with the timescales of the atmospheric ISV in the region. Active monsoon is clearly correlated with positive and negative phases of the ISV of latent-heat flux in the SCS. The characteristics of the intraseasonal latent-heat flux variations in summer are remarkably different from those in winter. The amplitudes of significant intraseasonal oscillations are about 35 and 80 $\text{W}\cdot\text{m}^{-2}$ during summer and winter monsoons, respectively. In summer, the intraseasonal latent-heat flux perturbations are characterized by slow eastward (about 1° latitude/day) and slower northward (about 0.75° longitude/day) propagations, probably in a response to eastward and northward propagating Madden-Julian oscillations (MJOs) from the equatorial Indian Ocean. In contrast, the perturbations appear to remain in the northern SCS region like a quasi-stationary wave in winter. In summer, the intraseasonal latent-heat flux fluctuations are highly correlated with wind speed. In winter, however, they are primarily associated with winds and near-surface air humidity. In addition, the intraseasonal SST variation is estimated to significantly reduce the amplitude of the intraseasonal latent-heat flux by 20% during winter.

1 Introduction

The South China Sea (SCS) is located on the southwest side of the North Pacific Ocean ($99\text{--}121^\circ$ E, $0\text{--}23^\circ$ N; Fig. 1a). The SCS climate is an important part of the Asian monsoon system. Basin-wide surface circulation changes drastically, depending on the season: cyclonic (anticyclonic) circulation develops in winter (summer) under the northeasterly (southwesterly) monsoon (e.g., Hu et al. 2000). The Asian summer monsoon, on the other hand, is known to display a wide variety of intraseasonal variability (ISV; Lau and Waliser 2005; Wang 2006). Since the atmospheric ISV was first shown by Madden and Julian (1971, 1972), its evolution and structure have been detailed by many composite studies (e.g., Rui and Wang 1990; Seo and Kumar 2008). Indeed, because ISV is characterized by timescales long enough to interact with the upper ocean, ISV has been linked to sea surface temperature (SST) variations in the Indian and Pacific Oceans (Zhang 1996; Saji et al. 2006; Han et al. 2007).

Just like ISV reported in the Indian and west Pacific Oceans, much of the interest in ISV has concerned at SST and winds in the SCS in recent years. Gao and Zhou (2002) demonstrated that characteristics of summer ISV in SST are remarkably different from those in winter. They suggested that intraseasonal SST fluctuations in summer were highly correlated to zonal wind and outgoing longwave radiation; however, they were primarily associated with meridional wind in winter. Xie et al. (2007a) described the life cycle of summer ISV in SST in the western SCS. Xie et al. (2007b) investigated summer ISV in wind jet, cold filament, and recirculations in the SCS. Their analysis showed that the developments of the wind jet and cold filament were not a smooth seasonal process but consisted of several intraseasonal events each year at about 45-day intervals. The intraseasonal cold filaments appeared to reduce the local

L. Zeng · D. Wang (✉)
Key Laboratory of Tropical Marine Environmental Dynamics,
South China Sea Institute of Oceanology,
Chinese Academy of Sciences,
164 West Xingang Road,
Guangzhou 510301, China
e-mail: dxwang@scsio.ac.cn

surface wind speed due to the increased static stability in the near-surface atmosphere. Using a cross-wavelet analysis for the SST off the Vietnam coast and a MJO index, Isoguchi and Kawamura (2006) revealed significantly large covariance at periods of 30–60 days in the summers of 2000–2002.

Until recently, limited information has been provided about the ISV in the associated surface fluxes. Krishnamurti et al. (1988) examined the global distribution of latent and sensible heat fluxes and SST variations on timescales of 30–50 days. They showed that the regions of pronounced ISV in SST lay over the tropical western Pacific Ocean and eastern Indian Ocean. Zhang and McPhaden (1995) and Zhang (1996) investigated the ISV of surface fluxes and SST using extended records of observations in the equatorial western Pacific (Hayes et al. 1991). They found that intraseasonal SST anomalies generally lagged reduced evaporation by about one-quarter cycle and thus concluded that latent-heat flux anomalies were primarily responsible for driving SST anomalies on the intraseasonal timescale. The principal surface heat flux terms on intraseasonal timescales are latent-heat flux and shortwave radiation, which varies mostly due to the cloudiness associated with convective systems.

Thanks to the influence of winds, shortwave and latent-heat flux terms are approximately in phase on intraseasonal timescales (Shinoda et al. 1998). The seasonal variability of latent-heat flux in the SCS is significant. The patterns of the seasonal-mean latent-heat flux follow more closely those of wind and humidity differences in winter. The pattern of seasonal latent-heat flux, however, follows more closely those of winds in summer (Zeng et al. 2009a). Therefore, studies are needed to examine in detail the temporal and spatial structures of intraseasonal latent-heat flux in the SCS. In addition, the periodicity of intraseasonal process has not been studied thoroughly. The purpose of this study is to examine the evolution of ISV associated with latent-heat flux and to investigate the difference in the propagation characteristics during summer and winter. We will address the following questions. (1) Is the ISV in latent-heat flux significant in the SCS? (2) What are the spatial structures of the intraseasonal latent-heat flux processes? (3) The ISV in latent-heat flux may simply be a response to ISV in some related variables. Is there any explicit relationship between the intraseasonal latent-heat flux signals and those related variables?

To address these issues, composite maps will be analyzed using proxy data for strong intraseasonal latent-heat flux events. The organization of the paper is as follows. Data and methodology are introduced in Section 2. The ISV in latent-heat flux is investigated in Section 3 through harmonic analysis, power spectrum variance analysis, and composite analyses. Section 4 explores intra-

seasonal latent-heat flux and variability of some related variables in the SCS using a lag regression analysis. Section 5 gives a summary and discussion of the results.

2 Data and methodology

As we know, latent-heat flux can be calculated based on wind speed (U), sea surface specific humidity (Q_s) that can be obtained from SST, and surface air humidity (Q_a). Launched in November 1997, the Tropical Rainfall Measuring Mission (TRMM) Microwave Imager (TMI) is a passive microwave sensor with a suite of channels ranging from 10.7 to 85 GHz that measures microwave energy emitted by the Earth and its atmosphere to quantify important atmospheric variables. Liu (1986) derived a global correlation between the monthly mean Q_a and total precipitable water based on the monthly atmospheric soundings. The relationship has been applied to compute ocean surface latent-heat flux and to study ocean's response to surface thermal forcing (e.g., Liu and Xie 1999). In the SCS, the relationship had been further verified by instantaneous sounding measurements and moored buoy observations (Zeng et al. 2009b). Based on Liu's relationship and TMI variables of SST, U and total precipitable water, Zeng and her collaborators calculated the latent-heat flux in the SCS (hereafter TMI latent-heat flux) using the Coupled Ocean–Atmosphere Response Experiment algorithm (COARE 3.0; Fairall et al. 2003). The TMI latent-heat flux has higher spatial resolution and more realistic values over the SCS basin than those from the Objectively Analyzed air-sea heat Fluxes (OAFlux; Yu et al. 2004), version 2 of the Goddard Satellite-based Surface Turbulent Fluxes (GSSTF2; Chou et al. 2003), the Japanese Ocean Flux Data Sets with use of Remote Sensing Observations (J-OFURO; Kubota et al. 2002), the National Centers for Environmental Prediction/Department of Energy reanalysis 2 (NCEP2; Kanamitsu et al. 2002) and the operational system of the European Centre for Medium-Range Weather Forecasts (ECMWF; Courtier et al. 1998). The TMI latent-heat flux has the highest correlation and the highest accuracy through the comparison with observations from mooring stations and buoys over the SCS. The mean root-mean-square (RMS) differences of the TMI latent-heat flux, OAFlux, GSSTF2, J-OFURO, NCEP2, and ECMWF with respect to observations are 27.4, 43.4, 45.7, 40.5, 39.6, and 59.7 $W \cdot m^{-2}$, respectively.

In this study, we use the $0.25 \times 0.25^\circ$ gridded TMI latent-heat flux from 10 January 1998 to 30 December 2006. We choose weekly mean data to suppress synoptic disturbances. The intraseasonal anomalies are isolated using a 30- to 90-day band-pass filter. Such a filter is commonly used in ISV studies and appropriate for the SCS, which, as will be

seen, has typical timescales of 5–8 weeks. Here, SCS summer is defined as June to August, and winter as December to February of the following year.

3 ISV of latent-heat flux

We begin with harmonic analysis to introduce the intraseasonal phenomenon of latent-heat flux in the SCS, followed by variance and composite analyses to extract its spatiotemporal characteristics.

3.1 Harmonic analysis

Harmonic analysis is used to investigate mainly oscillations of latent-heat flux in the SCS. The rectangular box in Fig. 1a indicates the area where the latent-heat flux time series is calculated. We compute $F_k = \frac{C_k^2/2}{2(s^2 - C_k^2)/(n-2-1)}$ to see if the k th harmonic wave is significant, where k is the harmonic wave number, C_k is the amplitude of k th harmonic wave, s^2 is the variance of time series, n is number of the total sample, and F_k is the F distribution whose df varies between 2 and $n-2-1$. The fourth to 14th (26–91 days) waves are all part of the ISV. In this study, we have either 52 or 53 weeks in each year. According to the table of F test, the given confidence level is 3.18. Thus, if the calculated F_k is greater than 3.18, the k th harmonic wave is significant (shaded regions in Fig. 1b).

As shown in Fig. 1b, the annual and semiannual cycles are the main periods, like mainly other variables in the SCS (Wang et al. 1997). Shaded areas indicate that the ISV of latent-heat flux (marked by a thick black line below the x axis) is also significantly strong in almost every year. The power is not so strong in 2001 and 2005 as in other years. The corresponding power spectra are given in Fig. 1c. The thick dashed line distinguishes variations greater than the 95% confidence level for a red-noise process (Torrence and Compo 1998). It shows explicit 30- to 90-day variations with two spectral peaks between 28–35 and 49–56 days.

3.2 Variance analysis

The intensity and spatial coherence of latent-heat flux ISV in the SCS are so striking that they can be identified even from unfiltered data. Figure 2 illustrates this with a time series of unfiltered latent-heat flux averaged over the longitudes of the box in Fig. 1a. Subseasonal variations of latent-heat flux are readily seen, punctuating the annual rise from summer to winter. The most pronounced intraseasonal event took place in January 2002, when the latent-heat flux increased from 46.7 to 144.0 $\text{W}\cdot\text{m}^{-2}$ in

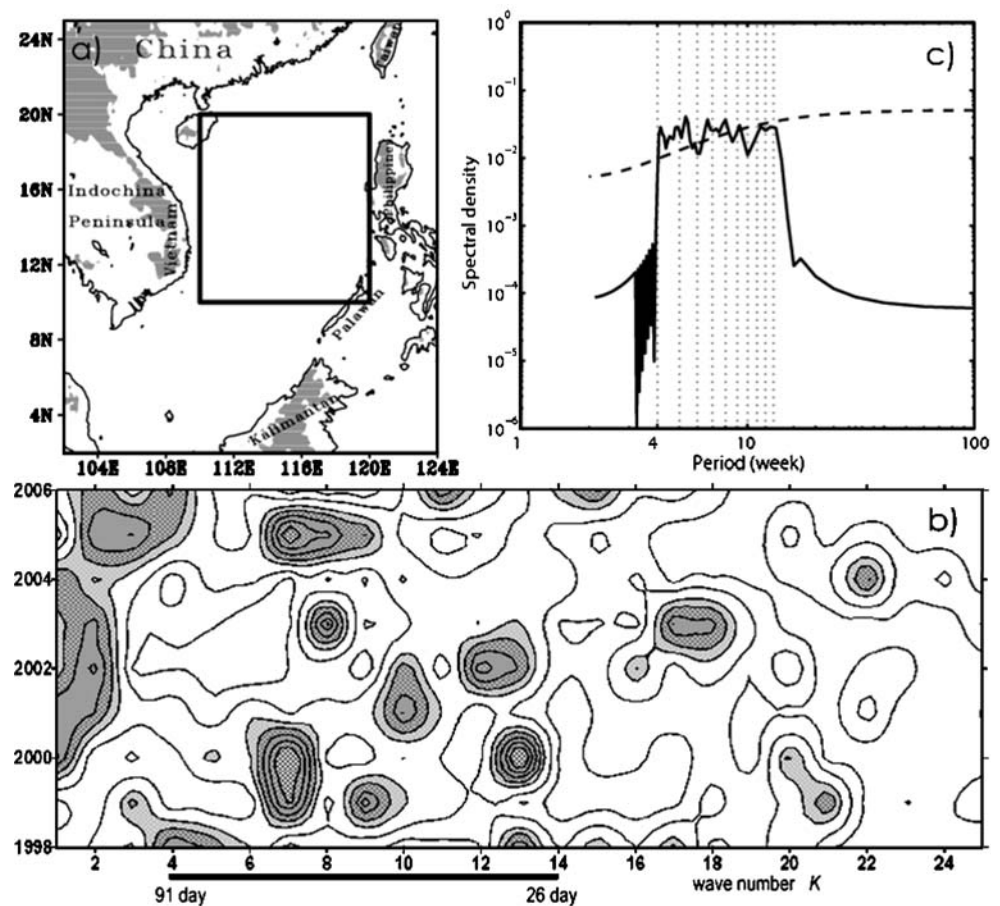
about 10 days and decreased to 73.1 $\text{W}\cdot\text{m}^{-2}$, 21 days after it reached the peak value. The amplitude of such an intraseasonal event is comparable to the seasonal change from summer to winter in any given year. From Fig. 2, we can see that negative and positive latent-heat flux anomalies occur alternatively in both summer and winter monsoon seasons. There is a significant difference in amplitude between the intraseasonal events in summer and winter. The amplitude of some winter intraseasonal events can even reach 80 $\text{W}\cdot\text{m}^{-2}$, while the maximum amplitude of the summer events is about 35 $\text{W}\cdot\text{m}^{-2}$. Stronger interannual variability also can be seen in winter than in summer. There is a weak northward propagation in summer intraseasonal events, while that in winter almost shows no propagation. Different from those in summers, stronger intraseasonal signals in winters seem to be trapped in the northern SCS.

Figure 3a and b show the standard deviations of 30–90 day latent-heat flux during summer and winter. In summer (Fig. 3a), it indicates relatively strong variability in the central SCS. Off the Southwest Vietnam coast, coinciding with the South Vietnam eddy (Wang et al. 2006), SDs exceed 23 $\text{W}\cdot\text{m}^{-2}$. In the eastern basin, high deviation exhibits the influence of strong winds and warm sea surface. The southwesterly summer monsoon seems to be the primarily cause for the large variance of intraseasonal latent-heat flux in the southern and eastern SCS. Other relatively active areas seem to be confined along the coastal areas of China.

Stronger ISV events of latent-heat flux tend to concentrate in winter (Fig. 3b). The SDs in the entire basin is large and varies from 20 to 60 $\text{W}\cdot\text{m}^{-2}$. The SDs exceed 30 $\text{W}\cdot\text{m}^{-2}$ in the northern two thirds of the basin, but individual events can produce peak to trough drops of as much as 97.3 $\text{W}\cdot\text{m}^{-2}$ (Fig. 2). In the southern region, the latent-heat flux variance decreases to 20 $\text{W}\cdot\text{m}^{-2}$. In the north, there is a large deviation tongue ($>45 \text{ W}\cdot\text{m}^{-2}$) extending southwestward from the Luzon Strait along the continental slope south of China. This large deviation tongue corresponds well with the prevailing northeasterly wind and surface cooling, indicative of distinct influence of the cold surges associated with the northeasterly winter monsoon. Coinciding with the West Luzon Eddy (Qu 2000), we see another maximum deviation core ($>50 \text{ W}\cdot\text{m}^{-2}$) centered at 120° E and 19° N. This core reflects large air–sea humidity difference induced by dry descending flow over the cold cyclonic eddy.

Power spectrums of summer and winter ISV signals of latent-heat flux are given in Figs. 3c and d. During summer, they reveal intraseasonal features with peak energy at a period of 35 days and display a weaker peak at 49–56 days; during winter, ISV with periods of 35–42 days is the most evident. This indicates that low frequency ISV presented earlier in Fig. 1b occurs mainly in summer.

Fig. 1 **a** Map of the SCS. The rectangular box (110–121° E, 10–20° N) indicates an area where the latent-heat flux time series is calculated. Geographical features cited in the text are shown; **b** Harmonic wave significant test of intraseasonal cycles from 1998 to 2006, using latent-heat flux averaged over the box marked in Fig. 1a. Abscissa count stands for the k th wave (k , 1–25) and time (year, 1998–2006), and ordinate for corresponding F value. Shaded waves are statistically significant at the 95% confidence level based on F test. The band in (26–91) days is indicated by a black line beneath the wave-numbers; **c** Power spectrum of intraseasonal latent-heat from 1998 to 2006 over the box marked in Fig. 1a. The solid line represents the power spectral density, and the dashed line is the 95% significant level; thin dashed line denotes the 28–91 day variability



3.3 Composite evolution

To map the structure of intraseasonal latent-heat flux events and their relationship with other atmospheric and oceanic variability, we performed a composite analysis based on an ISV index defined as latent-heat flux anomalies averaged in the rectangular box in Fig. 1a. We also performed an empirical orthogonal functions (EOFs) analysis of intraseasonal latent-heat flux variability and found that the first principal component is highly correlated with the index. Figure 4 shows that the intensity of some intraseasonal processes was comparatively strong. Consistent with Figs 2 and 3, the ISV during winter (thick shading in Fig. 4) is much stronger than that during summer (light shading).

Next, we track the evolution of latent-heat flux ISV by constructing lagged composite maps based on this index. Individual intraseasonal events are identified by applying the following criteria: (1) as intraseasonal event passes through the marked box in Fig. 1a, the box-averaged latent-heat flux anomaly should undergo a minimum and a maximum during the event, and (2) the minimum (maximum) value of the filtered box-averaged latent-heat flux anomaly is smaller (larger) than the SD value ($\pm\sigma$; $\sigma=15.6 \text{ W}\cdot\text{m}^{-2}$). The cases selected by the criteria are used for the composites for strong intraseasonal events. Since the SCS is located in the

monsoon system, we construct composite maps for summer and winter seasons separately. Thus, for the composite analysis, four strong summer intraseasonal events (12 Jun–14 Aug 1999, 26 May–07 Jul 2001, 08–20 Jul 2002, 10 Jun–22 Jul 2006; marked by gray upward-triangles) and ten strong winter events (09 Jan–27 Feb 1999, 27 Nov 1999–01 Jan 2000, 01 Jan–05 Feb 2000, 02 Dec 2000–13 Jan 2001, 13 Jan–24 Feb 2001, 01 Dec 2001–12 Jan 2002, 12 Jan–16 Feb 2002, 14 Dec 2002–01 Feb 2003, 27 Nov 2004–22 Jan 2005, 10 Dec 2005–28 Jan 2006; marked by dark downward-triangles) are chosen. The typical period of these distinct events in the SCS is 7 weeks (~ 49 days) in winter, and 8 (~ 56 days) weeks in summer.

The compositing technique employed here is similar to that of Gao et al. (2000). Each process was divided into nine stages. Stages 0 and 4 are balanced states of the selected process, and stage 8 is assumed to be identical to stage 0; stage 2 is assigned to the largest negative value, stage 6 to the largest positive value; the others occupy intermediate phases. A phase difference of 45° is nominally equivalent to a time difference of about 7 days.

Figure 5 presents the composite anomalies of intraseasonal latent-heat flux (color) and related variables (contour) from stages 1 to 6. Relatively strong ISV events mainly happened in the central and eastern SCS. The

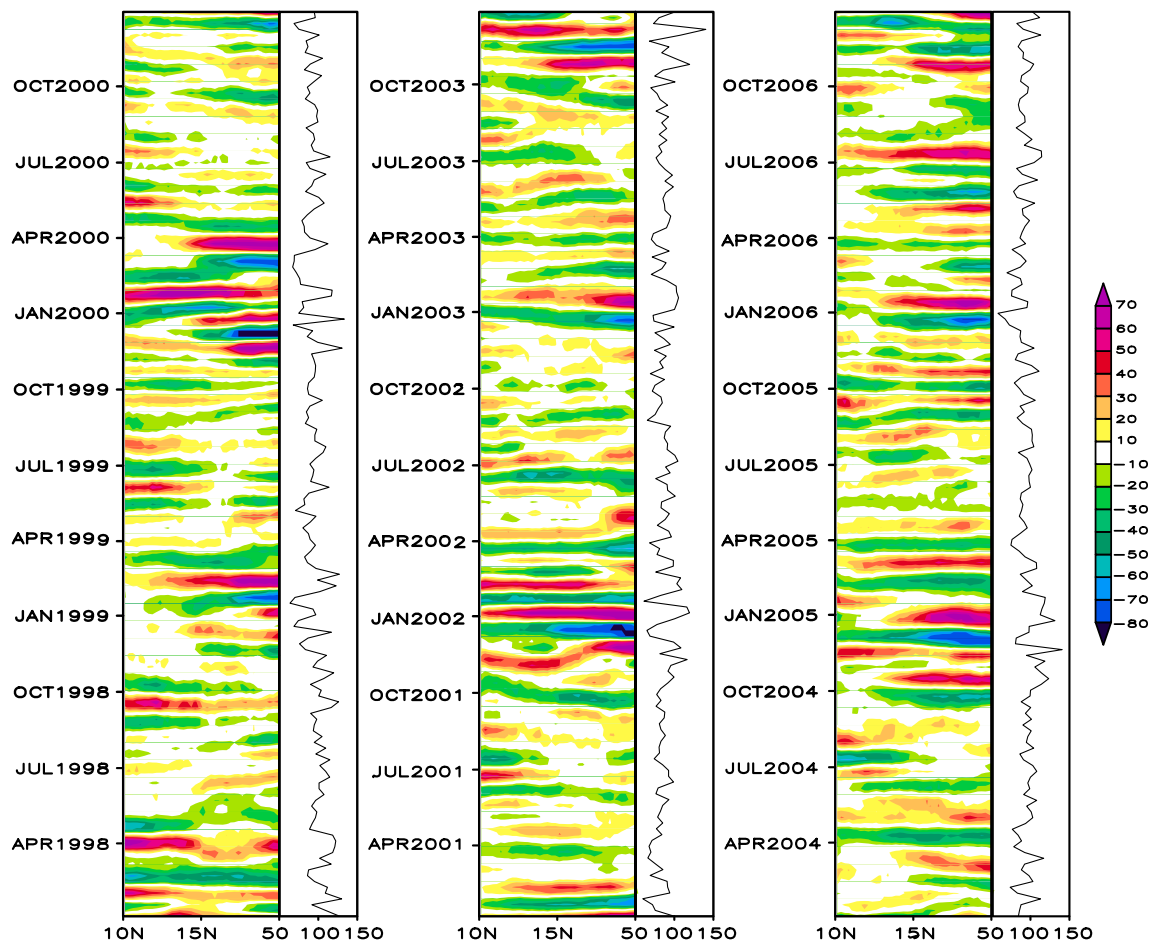


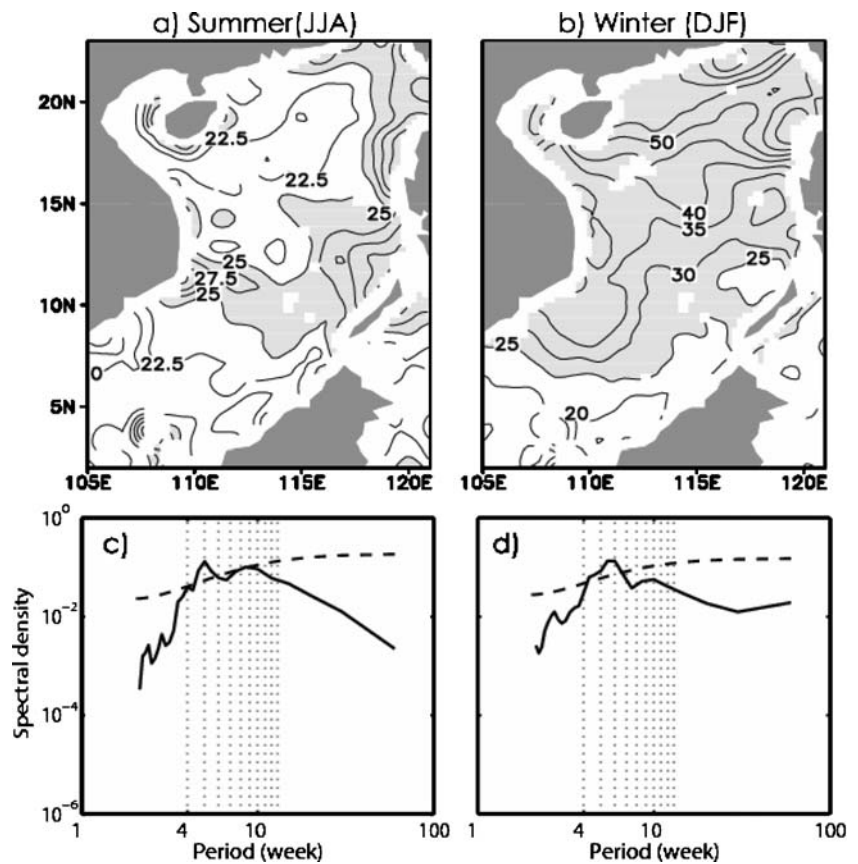
Fig. 2 Latitude–time plot of intraseasonal latent-heat anomaly ($\text{W}\cdot\text{m}^{-2}$) averaged between 110° E and 120° E and time series of area-averaged unfiltered latent-heat averaged over the box marked in Fig. 1a

intraseasonal latent-heat flux events during summer have mean amplitudes of $30 \text{ W}\cdot\text{m}^{-2}$, which is similar to the results of Krishnamurti et al (1988). At the initial phase (stage 0), averaged latent-heat flux in the SCS was in a state of equilibrium. Winds are calm, and SST is below the climatology. At the decay phase (stage 1), the southwesterly winds weaken by $0.25 \text{ m}\cdot\text{s}^{-1}$, and Q_a intensifies by $0.3 \text{ g}\cdot\text{kg}^{-1}$. Latent-heat flux of the whole basin decreases rapidly by $10\text{--}20 \text{ W}\cdot\text{m}^{-2}$ in response to this intraseasonal wind and humidity pulse. After that, at the peak phase (stage 2), the negative band continues to extend to the north, and latent-heat flux reaches the lowest value ($-30 \text{ W}\cdot\text{m}^{-2}$) between 10° N and 15° N. Wind pulse weakens and reaches the minimum, large wind anomalies of $1.5 \text{ m}\cdot\text{s}^{-1}$ are found west off the Philippines. On the other hand, Q_a anomalies strengthen to $0.6 \text{ g}\cdot\text{kg}^{-1}$ east of the South Vietnam. Then latent-heat flux anomalies start to increase in the following stages, reach its equilibrium state at stage 4, and turn positive in the following stages. At stage 4, latent-heat flux of the whole basin increases quickly, opposite to that in the previous period, and a positive core

emerges in the southeastern basin first. At the growth phase (stage 5), wind anomalies strengthen rapidly by $0.5 \text{ m}\cdot\text{s}^{-1}$ in the southern basin. At the same time, air humidity anomalies fall negative. In response to these intraseasonal oscillations, latent-heat flux intensifies rapidly by $20 \text{ W}\cdot\text{m}^{-2}$. At the peak phase (stage 6), latent-heat flux anomalies strengthen in the central eastern basin, maximized at $35 \text{ W}\cdot\text{m}^{-2}$ around 115° E and 15° N, with a distinct development of southwesterly wind band from southwest to northeast. Then latent-heat flux decreases and reaches to its equilibrium again, to complete the whole intraseasonal oscillation process of latent-heat flux. The amplitude of the composite SST, U , and Q_a variations associated with the latent-heat flux ISV in summer are 0.3°C , $1.75 \text{ m}\cdot\text{s}^{-1}$, and $0.3 \text{ g}\cdot\text{kg}^{-1}$, respectively.

Figure 6 presents the winter composite in stages 1 to 6. The zonally distributed intraseasonal latent-heat flux in winter is entirely different from that in summer. Coinciding with northeasterly winds during winter, negative and positive latent-heat flux anomalies all occur in the northern basin earlier. In stage 2, the basin attains its strongest negative phase. Associated with weak winds and largest

Fig. 3 The SD of intraseasonal latent-heat flux ($\text{W}\cdot\text{m}^{-2}$). **a** Summer (June–July–August; interval $2.5 \text{ W}\cdot\text{m}^{-2}$) and **b** winter (December–January–February; interval $5 \text{ W}\cdot\text{m}^{-2}$). **c, d** For intraseasonal latent-heat during summer and winter, respectively



Q_a is the minimum amplitude of latent-heat flux band ($< -50 \text{ W}\cdot\text{m}^{-2}$) north of 20° N . After the calm winds and reduced latent-heat flux, the ocean warms up by 0.1°C . At stage 4, positive latent-heat flux anomalies first appear west off the Philippines. Following its equilibrium state, latent-heat flux of the northern basin increases quickly and attains its highest value in stage 6. Opposite to stage 2, the basin has its maximum in the northern SCS, indicating the contribution of cold and dry airs brought by cold surges. The enhanced northeasterly winds (by $1 \text{ m}\cdot\text{s}^{-1}$) and rapidly decreased Q_a (by $1.5 \text{ g}\cdot\text{kg}^{-1}$) both accelerate the development of the latent-heat flux oscillations by $50 \text{ W}\cdot\text{m}^{-2}$ in the northern SCS. The strength of the intraseasonal processes in winter monsoon season is much stronger than that in summer monsoon season, consistent with the results discussed earlier.

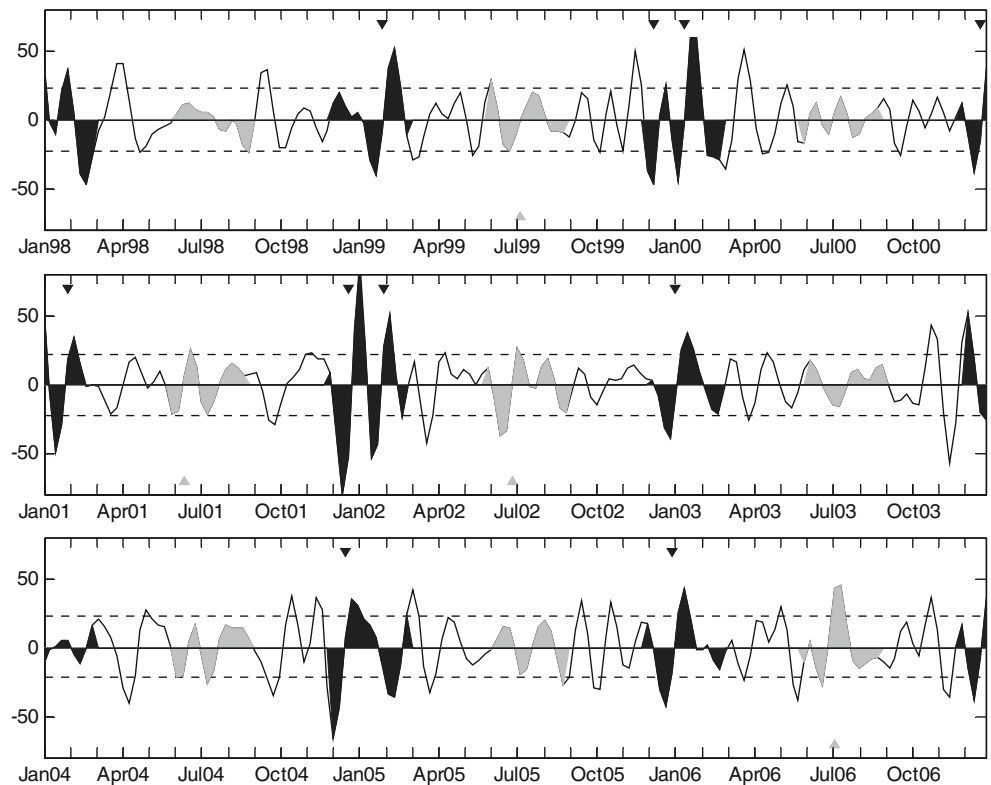
From Figs. 5 and 6, we can see that winds, humidity, and latent-heat flux all seem to be in phase most of the time. Surface winds affect SST by altering latent-heat flux and induced entrainment cooling. Reduced latent-heat flux and cooling can warm up the surface ocean. Note that the minimum wind contours appear about two stages (~ 10 days) before the maximum SST. This is because it is the time derivative (or change) of SST, rather than the SST itself, which is directly proportional to the turbulent heat flux and entrainment cooling. As a result, SST often lags winds and

latent-heat flux, which is consistent with previous studies (Zhang and McPhaden 1995; Han et al. 2007).

4 Effect of intraseasonally varying variables on latent-heat flux

In order to get a full insight into the spatial distribution in each stage, we made a latitude–time diagram (averaged over $105\text{--}121^\circ \text{ E}$) and a longitude–time diagram (averaged over $2\text{--}23^\circ \text{ N}$) for intraseasonal latent-heat flux in summer (Figs. 7a and e) and winter (Fig. 8a and e), respectively. The amplitude in winter is larger in latitude–time section ($55 \text{ W}\cdot\text{m}^{-2}$) and longitude–time section ($35 \text{ W}\cdot\text{m}^{-2}$) than in summer ($25 \text{ W}\cdot\text{m}^{-2}$). In the latitude–time section for summer (Fig. 7a), the northward propagation is seen from 8° N to 16° N . The average northward propagation speeds is about $0.75^\circ/\text{day}$. In the longitude–time section, there is a relatively fast eastward propagation, about $1^\circ/\text{day}$, east of 110° E (Fig. 7e). These summer intraseasonal oscillations are probably responses to eastward and northward propagating Madden-Julian Oscillations (MJOs) from the equatorial Indian Ocean (e. g., Rui and Wang 1990). Figure 8a and e shows that intraseasonal latent-heat flux in winter is almost without any zonal or meridional propagation, which means that the ISV of latent-heat flux in winter is just like a

Fig. 4 Time series of averaged intraseasonal latent-heat flux anomalies averaged over the box marked in Fig. 1a, from 1998 to 2006. Unit is $W \cdot m^{-2}$. The dotted line denotes the $Sd (\pm\sigma; \sigma=15.6 W \cdot m^{-2})$. Variability during summer (winter) is light shaded (thick shading). In summer (winter), four (ten) distinct intraseasonal events greater than the SD are marked by gray upward triangles (black downward triangles). Each event is divided into nine stages. Stages 0 and 4 are balanced states of the selected process, stage 2 is assigned to the largest negative value, and stage 6 to the largest positive value



quasi-stationary wave. This suggests that once intraseasonal latent-heat flux variability occurs at the surface, heat condition in the whole SCS responds to it rapidly. As shown in Fig. 8a, strong intraseasonal latent-heat flux signals in winter are trapped in the northern SCS, consistent with Fig. 2.

The composite analyses indicate that the typical swings in related variables, such as SST, U , and Q_a , associated with the passage of the intraseasonal latent-heat flux is about $0.3^\circ C$, $1.75 m \cdot s^{-1}$, and $0.3 g \cdot kg^{-1}$ in summer, and $0.3^\circ C$, $1.0 m \cdot s^{-1}$, and $1.9 g \cdot kg^{-1}$ in winter. One important question is whether such an ISV can significantly affect the intraseasonally varying latent-heat flux. The moisture flux due to the SST variation may significantly change the moisture content in the atmospheric boundary layer, and this may initiate the deep convection. The impact of a $0.3^\circ C$ change in SST on the latent-heat flux can be estimated using the standard bulk formula, assuming that U and Q_a remain constant as the SST increases. These changes are estimated as

$$Q_{LH} = \rho_a L_e C_e U (Q_s - Q_a)$$

where Q_{LH} is the latent-heat flux, ρ_a is the air density, C_e is the exchange coefficients, L_e is the latent-heat of vaporization. SST change from $29.0^\circ C$ to $29.3^\circ C$ corresponds to a humidity increase of $0.44 g \cdot kg^{-1}$. For a U equal to $4 m \cdot s^{-1}$, the latent-heat flux increases by $6.7 W \cdot m^{-2}$. Here we have used $C_e=1.3 \times 10^{-3}$, $\rho_a=1.2 kg \cdot m^{-3}$, and $L_e=2,441 W \cdot s \cdot g^{-1}$.

These increases are significant considering that the amplitude of the composite latent-heat flux variation associated with intraseasonal variation is about $30 W \cdot m^{-2}$ in the SCS. On the other hand, changes by $0.3 g \cdot kg^{-1}$ ($1.9 g \cdot kg^{-1}$) of Q_a in summer (winter) would bring latent-heat flux of about $4.6 W \cdot m^{-2}$ ($28.9 W \cdot m^{-2}$). For wind change, the increase of U by $1.75 m \cdot s^{-1}$ in summer ($1.0 m \cdot s^{-1}$ in winter) is estimated to build up the amplitude of the latent-heat flux by $33.3 W \cdot m^{-2}$ ($19.0 W \cdot m^{-2}$). This simple estimation suggests the possibility that northeasterly monsoon and associated cold dry air affect the evolution of latent-heat flux ISVs during winter. On the other hand, the force of southwesterly monsoon is probably significant during summer. More detailed behavior of these parameters will be discussed next.

A more accurate estimate of the impact of the intraseasonally varying SST, U , and Q_a on the latent-heat flux ISV is to recompute latent-heat flux using these three variables from which the intraseasonal variations have been removed. Take SST for example, we do this by low-pass filtering the SST (via spectral transformation) to periods longer than 120 days. Hence, the seasonal cycle and longer timescales are retained, whereas the intraseasonal variations are removed. To isolate the impact of just the intraseasonally varying SST, U , and Q_a calculated from the original weekly SST, only SST and Q_s are from the low-pass-filtered SST. From Fig. 7b and e, we can see that the difference is neglectable in summer if ISV of SST is

Fig. 5 Temporally varying summer composite intraseasonal latent-heat anomalies ($\text{W}\cdot\text{m}^{-2}$). *Shadings* indicate latent-heat flux anomalies that are statistically significant at the 95% level, based on their local SDs and the Student's *t* test) and related variables (contours) from stages 1 to 6. **a–f** SST (interval $0.1\text{ }^{\circ}\text{C}$); **g–l** wind speed (*U*; interval $0.25\text{ m}\cdot\text{s}^{-1}$); **m–r** near-surface air humidity (Q_a ; interval $0.1\text{ g}\cdot\text{kg}^{-1}$)

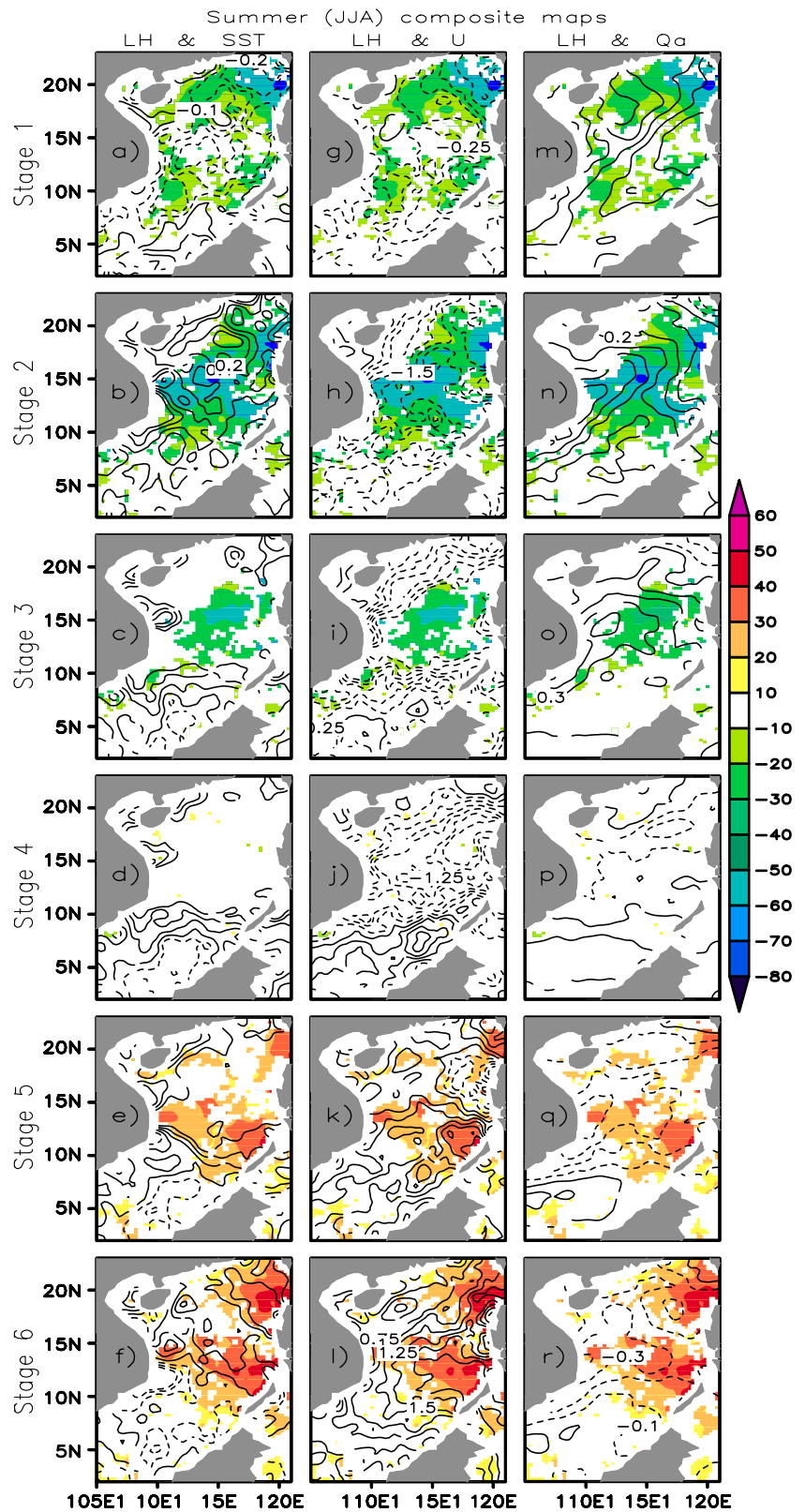


Fig. 6 Same as Fig. 5, except for winter composite events

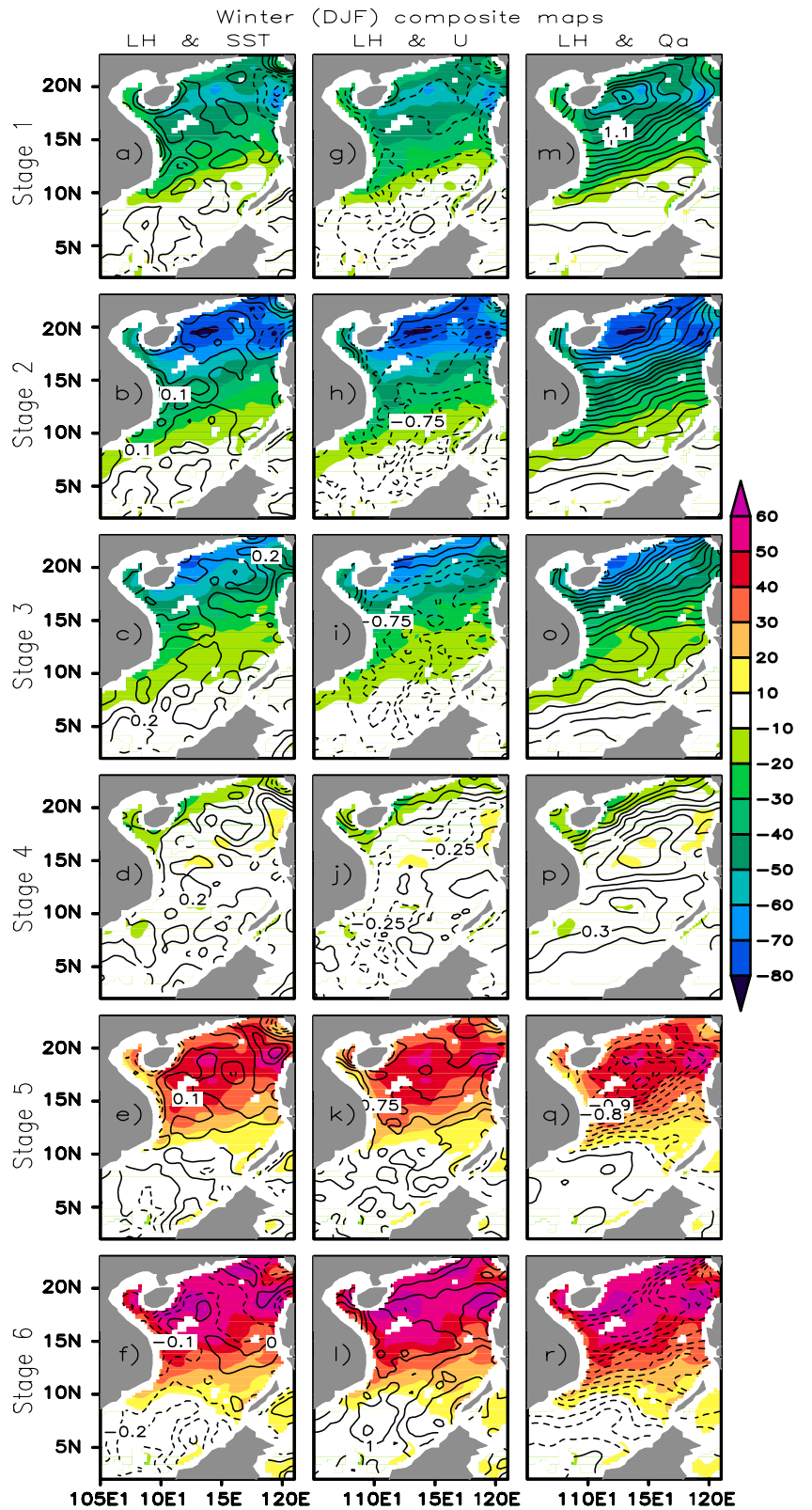
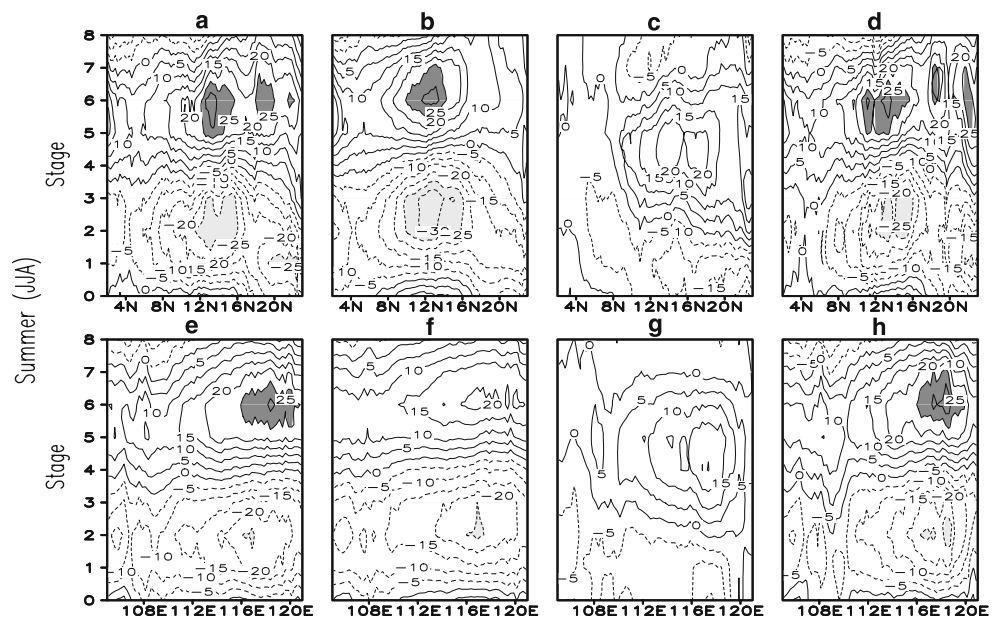


Fig. 7 Latitude–time diagram (averaged over 105–121° E) of summer composite intraseasonal latent-heat based on weekly variables (**a**) and based on low-pass-filtered variables; **b** low-pass-filtered SST; **c** low-pass-filtered U ; **d** low-pass-filtered Q_a . **e–h** same as (**a–d**) but for longitude–time maps

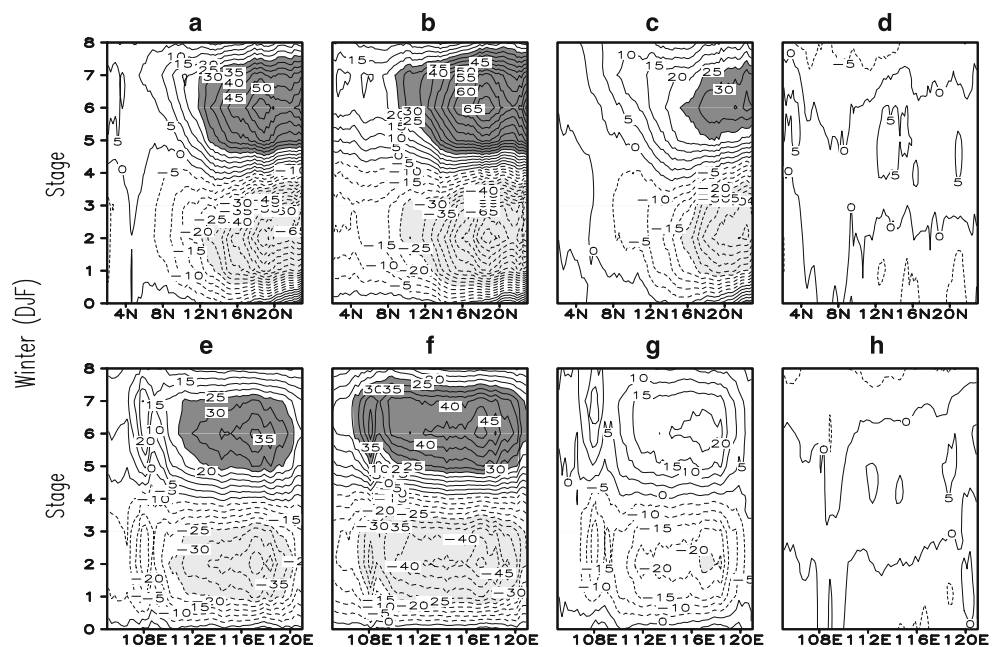


removed. We also recompute the latent-heat flux with the low-pass-filtered winds and Q_a . As it shown in Fig. 7c and g, spatial and propagation characteristics of summer intraseasonal latent-heat flux are dominated by the southwesterly winds. While the ISVs of winds have been removed during summer, the latent-heat anomalies precede about 10 days.

During winter (Fig. 8b and e), the amplitude of the composite latent-heat flux variation increases uniformly by about $10 \text{ W}\cdot\text{m}^{-2}$ when the low-pass-filtered SST is used in place of the weekly SST. Thus, the intraseasonal SST variation would reduce the amplitude of latent-heat flux by about 20%. Our result is consistent with Shinoda et al. (1998), who found that the intraseasonal SST variation is

estimated to significantly reduce the amplitude of the latent and sensible heat fluxes produced by the MJOs by 15%. The intraseasonal SST variation tends to reduce the amplitude of the latent-heat flux variation because the maximum intraseasonally varying winds tend to cause slightly colder SST. Hence, the correlation between the intraseasonally varying winds and SST is negative. As a result, inclusion of the intraseasonally varying SST acts to reduce the amplitude of the latent-heat flux over that computed with climatological SST. Although a $10\text{-W}\cdot\text{m}^{-2}$ change of the latent-heat flux variation is significant, its actual impact on the evolution of the intraseasonal oscillations awaits modeling studies that can faithfully account for this effect. Different from summer intraseasonal oscillations, the intraseasonal latent-heat flux

Fig. 8 Same as Fig. 7 except for composite winter events



variations in winter are mainly determined by northeasterly winds, and Q_a , and Q_a appears to make a greater contribution than winds. When the intraseasonal oscillations of Q_a are removed, the amplitude composite latent-heat flux is reduced to only $5 \text{ W}\cdot\text{m}^{-2}$.

5 Summary and discussion

The spatial and temporal characteristics of intraseasonal latent-heat flux variability in the SCS are examined using weekly data from January 1998 to December 2006. Harmonic analysis of latent-heat flux shows the time evolution of the dominant modes of seasonal and intraseasonal oscillation with 95% confidence level. Some fundamental features of the ISV in latent-heat flux are described. A typical intraseasonal latent-heat flux shows two spectral peaks at 28–35 and 49–56 days, comparable with the timescales of atmospheric intraseasonal events in the region (e.g., Straub and Kiladis 2003; Jiang et al. 2004).

Motivated by the assumption that different monsoonal processes might exert different influences over the latent-heat flux variability, we document our findings in summer and winter, respectively. The amplitudes of significant intraseasonal oscillations are about $35 \text{ W}\cdot\text{m}^{-2}$ ($80 \text{ W}\cdot\text{m}^{-2}$) in summer (winter). In summer, though relatively strong variability happens in the central and eastern basins, there is no large variability seen in the spatial pattern of the intraseasonal latent-heat flux. In winter, the spatial pattern of the intraseasonal latent-heat flux variations is zonally distributed and relatively trapped in the northern basin. The intraseasonal latent-heat flux variations in summer exhibit weak eastward and northward propagation throughout the SCS, with speeds of 1° and $0.75^\circ/\text{day}$, respectively. In winter, a quasi-stationary wave pattern suggests that once intraseasonal latent-heat flux variability occurs at the surface, heat condition in the whole SCS responds rapidly. These summer intraseasonal oscillations are probably responses to eastward and northward propagating MJOs from the equatorial Indian Ocean. In order to investigate possible interactions between the summer latent-heat flux and the MJO phenomena, we apply the MJO index proposed by Wheeler and Hendon (2004). Evolution of the MJOs along the equator can be described for all seasons using this index. High correlations between this MJO index and composite summer intraseasonal latent-heat flux signals further illustrate significant influence by the MJOs (figure is not shown).

The intraseasonal latent-heat flux fluctuations are highly correlated to southwesterly winds in summer, and primarily associated with northeasterly winds and Q_a in winter. In summer, onset of the southwesterly monsoon bring strong winds and warm surface in central and eastern SCS, strengthening the evolution of ISV in latent-heat flux. In

winter, cold and dry air streams associated with cold surges are favorable for the active intraseasonal latent-heat flux signals. The effects of ISV in SST, winds, and Q_a are further estimated by recomputing latent-heat flux using low-pass-filtered variables instead of weekly variables. During winter, SST variation of about 0.3°C due to the filtering of the intraseasonal SST is estimated to reduce the amplitude of the intraseasonal latent-heat flux by about 20%. This suggests the possibility that the time-varying SST may significantly affect the evolution of the convection, and hence, may play an important role in determining the characteristics of the MJOs. Therefore, better understanding of the air–sea interaction in the monsoon region, which is also recommended by Sengupta and Ravichandran (2001), is of great importance for giving further insight into the influence of latent-heat flux variations at intraseasonal timescales in this region and for identifying the differences from those in tropical oceans.

Acknowledgements TMI dataset was downloaded from the Remote Sensing Systems Company (www.ssmi.com). We thank Drs. Xin Wang, Ju Chen, and Wei Zhuang for the discussions. Constructive comments by three reviewers are gratefully acknowledged. This study was supported by the Chinese Academy of Sciences (KZSW2-YW-214), National Basic Research Program of China (no. 2006CB403604), and Natural Science Foundation of China under contract nos. U0733002, 40625017, and 40876007.

References

- Chou SH, Nelkin E, Ardizzone J, Atlas RM, Shie CL (2003) Surface turbulent heat and momentum fluxes over global oceans based on the Goddard satellite retrievals, version 2 (GSSTF2). *J. Climate* 16:3256–3273
- Courtier P, Andersson E, Heckley W, Pailleux J, Vasiljevic D, Hamrud M, Hollingsworth A, Rabier F, Fischer M (1998) The ECMWF implementation of three-dimensional variational assimilation (3D-Var). I: formulation. *Quart. J. Roy. Meteor. Soc.* 124B:1783–1808
- Fairall CW, Bradley EF, Hare JE, Grachev AA, Edson JB (2003) Bulk parameterization of air–sea fluxes: updates and verification for the COARE algorithm. *J. Climate* 16:571–591
- Gao RZ, Zhou FX (2002) Monsoonal characteristics revealed by intraseasonal variability of sea surface temperature in the South China Sea. *Geophys. Res. Lett.* 29(8):1222. doi:10.1029/2001GL014225
- Gao RZ, Zhou FX, Fang WD (2000) SST intraseasonal oscillation in the SCS and atmospheric forcing system. *Chinese J. Oceanol. & Limnol* 15:289–296
- Han WQ, Yuan DL, Liu WT, Halkides DJ (2007) Intraseasonal variability of Indian Ocean sea surface temperature during boreal winter: Madden–Julian Oscillation versus submonthly forcing and processes. *J. Geophys. Res.* 112:C04001. doi:10.1029/2006JC003791
- Hayes SP, Mangum LJ, Picaud J, Sumi A, Takeuchi K (1991) TOGA-TAO: a moored array for real-time measurements in the tropical Pacific Ocean. *Bull. Amer. Meteor. Soc.* 72:339–347
- Hu JY, Kawamura H, Hong HS, Qi YQ (2000) A review on the currents in the South China Sea-Seasonal circulation, South China Sea Warm Current and Kuroshio intrusion. *J. Oceanogr.* 56:607–624
- Isoguchi O, Kawamura H (2006) MJO-related summer cooling and phytoplankton blooms in the South China Sea in recent years. *Geophys. Res. Lett.* 33:L16615. doi:10.1029/2006GL027046

- Jiang X, Li T, Wang B (2004) Structures and mechanisms of the northward propagating boreal summer intraseasonal oscillation. *J. Climate* 17:1022–1039
- Kanamitsu M, Ebisuzaki W, Woollen J, Yang SK, Sling JJ, Fiorino M, Potter GL (2002) NCEP-DOE AMIP-II Reanalysis (R-2). *Bull. Amer. Meteor. Soc.* 83:1631–1643
- Krishnamurti TN, Dosterhof D, Mehta A (1988) Air–sea interaction on the time scale of 30–50 days. *J. Atmos. Sci.* 45:1304–1322
- Kubota M, Ichikawa K, Iwasaka N, Kizu S, Konda M, Kutsuwada K (2002) Japanese ocean flux data sets with use of remote sensing observations (J-OFURO). *J. Oceanogr.* 58:213–215
- Lau, WKM, Waliser DE (2005), *Intraseasonal variability of the atmosphere–ocean climate system.* 474 pp., Springer, Heidelberg, Germany
- Liu WT (1986) Statistical relation between monthly mean precipitable water and surface-level humidity over global oceans. *Mon. Wea. Rev.* 114:1591–1601
- Liu WT, Xie X (1999) Space-based observations of the seasonal changes of South Asian monsoons and oceanic response. *Geophys. Res. Lett.* 26:1473–1476
- Madden RA, Julian PR (1971) Detection of a 40–50 day oscillation in the zonal wind in the tropical Pacific. *J. Atmos. Sci.* 28:702–708
- Madden RA, Julian PR (1972) Description of global-scale circulation cells in the Tropics with a 40–50 days period. *J. Atmos. Sci.* 29:1109–1123
- Qu D (2000) Upper-layer circulation in the South China Sea. *J. Phys. Oceanogr.* 30:1450–1460
- Rui HL, Wang B (1990) Development characteristics and dynamic structure of tropical intraseasonal convection anomalies. *J. Atmos. Sci.* 47:357–379
- Saji NH, Xie SP, Tam CY (2006) Satellite observations of intense intraseasonal cooling events in the tropical south Indian Ocean. *Geophys. Res. Lett.* 33:L14704. doi:10.1029/2006GL026525
- Sengupta D, Ravichandran M (2001) Oscillations of Bay of Bengal sea surface temperature during the 1998 summer monsoon. *Geophys. Res. Lett.* 28:2033–2036
- Seo K, Kumar A (2008) The onset and life span of the Madden-Julian oscillation. *Theor. Appl. Climatol.* 94(1–2):13
- Shinoda T, Hendon HH, Glick J (1998) Intraseasonal variability of surface fluxes and sea surface temperature in the tropical western Pacific and Indian Oceans. *J. Climate* 11:1685–1702
- Straub KH, Kiladis GN (2003) Interactions between the boreal summer intraseasonal oscillation and higher-frequency tropical wave activity. *Mon. Wea. Rev.* 131:945–960
- Torrence C, Compo GP (1998) A practical guide to wavelet analysis. *Bull. Am. Meteor. Soc.* 79:61–78
- Wang B (2006) *The Asian Monsoon.* Springer, New York, p 787
- Wang DX, Zhou FX, Li YP (1997) Characteristics of sea surface temperature and surface heat budget on annual cycle time scales in the South China Sea. *Acta Oceanol. Sinica* 15:111–125
- Wang GH, Chen D, Su JL (2006) Generation and life cycle of the dipole in the South China Sea summer circulation. *J. Geophys. Res.* 111:C06002. doi:10.1029/2005JC003314
- Wheeler MC, Hendon HH (2004) An all-season real-time multivariate MJO index: development of an index for monitoring and prediction. *Mon. Wea. Rev.* 132:1917–1932
- Xie Q, Wu XY, Yuan WY, Wang DX, Xie S-P (2007a) Life cycle of intraseasonal oscillation of summer SST in the western South China Sea. *Acta Oceanol. Sinica* 3:1–8
- Xie S-P, Chang CH, Xie Q, Wang DX (2007b) Intraseasonal variability in the summer South China Sea: wind jet, cold filament, and recirculations. *J. Geophys. Res.* 112:C10008. doi:10.1029/2007JC004238
- Yu LS, Weller RA, Sun BM (2004) Improving latent and sensible heat flux estimates for the Atlantic Ocean (1988–1999) by a synthesis approach. *J. Climate* 17:373–393
- Zeng LL, Shi P, Liu WT, Wang DX (2009a) Intercomparison of various latent heat flux products in the South China Sea. *Adv. Geosciences (OS)* (in press)
- Zeng LL, Shi P, Liu WT, Wang DX (2009b) Evaluation of a satellite-derived latent heat flux product in the South China Sea: A comparison with moored buoy data and various products. *Atmos. Res.* doi:10.1016/j.atmosres.2008.12.007
- Zhang C (1996) Atmospheric intraseasonal variability at the surface in the tropical western Pacific Ocean. *J. Atmos. Sci.* 53:739–758
- Zhang GJ, McPhaden MJ (1995) The relationship between sea surface temperature and latent heat flux in the equatorial Pacific. *J. Climate* 8:589–605
- Zhou FX, Ding J, Yu SY (1995) The intraseasonal oscillation of sea surface temperature in the South China Sea. *J. Ocean Univ Qingdao (in Chinese)* 25:1–6